Available online at www.sciencedirect.com
ScienceDirect
Nuclear Instruments and Methods in Physics Research A 577 (2007) 117–124
NUCLEAR INSTRUMENTS & METHODS IN PHYSICS RESEARCH Section A
www.elsevier.com/locate/nima

Conditions for minimization of halo particle production during transverse compression of intense ion charge bunches in the Paul Trap Simulator Experiment (PTSX)

Erik P. Gilson[a,*], Moses Chung[a], Ronald C. Davidson[a], Mikhail Dorf[a], Philip C. Efthimion[a], David P. Grote[b], Richard Majeski[a], Edward A. Startsev[a]

[a]*Plasma Physics Laboratory, Princeton University, Princeton, NJ 08543, USA*
[b]*Lawrence Livermore National Laboratory, University of California, Livermore, CA 94550, USA*

Available online 22 February 2007

Abstract

The Paul Trap Simulator Experiment (PTSX) is a compact laboratory Paul trap that simulates propagation of a long, thin charged-particle bunch coasting through a multi-kilometer-long magnetic alternating-gradient (AG) transport system by putting the physicist in the frame-of-reference of the beam. The transverse dynamics of particles in both systems are described by the same sets of equations—including all nonlinear space-charge effects. The time-dependent quadrupolar voltages applied to the PTSX confinement electrodes correspond to the axially dependent magnetic fields applied in the AG system. This paper presents the results of experiments in which the amplitude of the applied confining voltage is changed over the course of the experiment in order to transversely compress a beam with an initial depressed tune $\nu/\nu_0 \sim 0.9$. Both instantaneous and smooth changes are considered. Particular emphasis is placed on determining the conditions that minimize the emittance growth and, generally, the number of particles that are found at large radius (so-called halo particles) after the beam compression. The experimental data are also compared with the results of particle-in-cell (PIC) simulations performed with the WARP code.

PACS: 29.27.−a; 41.85.Ja; 52.27.Jt

Keywords: Ion beam; Accelerator; Plasma; Paul trap

1. Introduction

It is important to develop an improved fundamental understanding of the influence of collective processes and self-field effects on the long-distance propagation of intense charged-particle beams through magnetic alternating-gradient (AG) transport systems [1–6]. This is motivated by the high beam intensities envisioned in present and next-generation facilities in fields such as heavy ion fusion, spallation neutron sources, high energy and nuclear physics, and ion-beam-driven high-energy density physics [7]. There is interest in fields such as fundamental nonlinear dynamics. The Paul Trap Simulator Experiment (PTSX) is an experimental facility that allows the propagation of intense charged particle beams over large distances to be studied in a compact and flexible laboratory experiment. Important scientific topics such as: beam mismatch and the dynamics of halo particles, conditions for quiescent propagation, collective mode excitation and control, and distribution function effects can be studied in PTSX [8–12].

In an intense charged particle beam, the effect of the beam's self-electric and self-magnetic fields cannot be neglected. The relative importance of these self-fields is described by the normalized intensity parameter $s = \omega_p^2/2\omega_q^2$, where $\omega_p^2 = n_b e_b^2/m_b\varepsilon_0$ is the plasma frequency-squared, which characterizes the strength of the self-fields, and ω_q is the average smooth-focusing frequency of the beam particles' transverse oscillations in the applied focusing field. Here, n_b, e_b, and m_b are the beam density,

*Corresponding author. Tel.: +1 609 243 2681.
E-mail address: egilson@pppl.gov (E.P. Gilson).

0168-9002/$ - see front matter © 2007 Published by Elsevier B.V.
doi:10.1016/j.nima.2007.02.042

particle charge, and particle mass, respectively. When $s \ll 1$, the beam is emittance dominated, while $s \to 1$ implies that the beam is space-charge dominated. For a flat-top density profile, the normalized intensity s and the depressed tune ν/ν_0 are related by $\nu/\nu_0 = (1-s)^{1/2}$.

A linear Paul trap [13] confining a one-component plasma can be used to simulate the fully self-consistent transverse dynamics of a long, thin, charge bunch in the beam frame of an AG system because the particles' equations of motion are the same [14,15]. In the beam frame of the AG system, the spatially oscillating magnetic quadrupole fields become transformed into temporally oscillating electric quadrupole fields that have the same form as the oscillating electric fields applied in a linear Paul trap. The self-electric and self-magnetic fields of a long thin beam bunch can be described by a single scalar potential that obeys Poisson's equation, while the self-electric field of a trapped plasma naturally obeys Poisson's equation. The single-particle Hamiltonians, and therefore the resulting Vlasov equations for the two systems also have similar forms.

The voltage waveform amplitude and frequency applied to the electrodes of PTSX therefore correspond to the magnet strength and lattice spacing in an AG system. The long confinement times of plasmas in PTSX and the arbitrary form of the computer-generated voltage waveform make PTSX a flexible facility for studying intense beam propagation.

A brief description of the PTSX facility is given in Section 2. Section 3 discusses the minimization of halo particles that are produced by the mismatch between the ion source and the transverse confinement lattice. Further optimization of the injected plasma is described in Section 4. In Section 5, the results of experiments are presented in which the applied voltage waveform amplitude is changed in order to intentionally create a mismatch. Throughout this paper, comparisons are made with particle-in-cell (PIC) simulations using the WARP code [16].

2. Paul Trap Simulator Experiment

Fig. 1 shows a sketch of PTSX. The PTSX device [17–21] is a linear Paul trap constructed from a 2.8-m-long, $r_w = 10$-cm-radius cylinder. The cylinder is divided into two 40-cm-long end cylinders and a $2L = 2$-m-long central cylinder. All cylinders are azimuthally divided into four 90° segments so that when an oscillating voltage $V_0(t)$ is applied with alternating polarity on adjacent segments, the resulting oscillating transverse quadrupole electric field exerts a ponderomotive force that confines the plasma radially. To trap the plasma axially, the two end cylinders are biased to a constant voltage $\hat{V}$. Voltage waveforms with amplitudes up to 400 V and frequencies up to 100 kHz can be used. The trapping voltage is nominally $\hat{V} = 36$ V. The vacuum pressure of 5×10^{-9} Torr prevents neutral collisions from playing an important role in the plasma behavior.

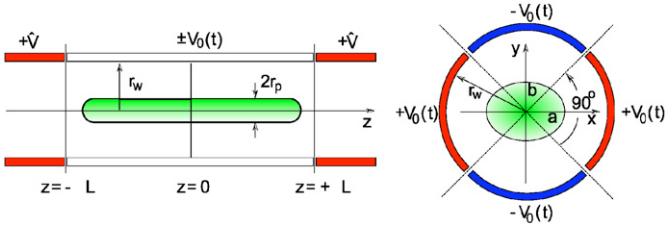

Fig. 1. PTSX is a cylindrical Paul trap that consists of a central confinement cylinder and a pair of shorter axial-trapping electrodes. The oscillating voltage applied to the four 90° segments creates a ponderomotive force that transversely confines the one-component cesium ion plasma.

The plasma source is a 1.5-cm-diameter aluminosilicate cesium emitter. Singly charged cesium ions are extracted by applying a bias of less than 10 V between the emitter and an "acceleration" grid. The ions then pass through a separately biased "deceleration" grid. The ion source is situated in the middle of one of the 40-cm-long cylinders, and to inject a pure cesium ion plasma into the trap, the segments on this 40-cm-long cylinder are temporarily set to oscillate with the voltage $\pm V_0(t)$. The injection time t_i is several milliseconds in order to allow cesium ions with several eV of kinetic energy to fill the trap.

After being trapped for a time t_t, that can be up to 300 ms, the 40-cm-long cylinder on the opposite end of PTSX from the ion source is set to oscillate with voltage $\pm V_0(t)$, and the plasma streams out of the trap. Part of the exiting plasma is collected on a moveable 5-mm-diameter collector disk. The inject–trap–dump cycle is repeated to reduce the uncertainty in the data. The collector is moved in the transverse plane in order to collect a radial density profile of the trapped plasma. Note that since the plasma ions can take several milliseconds to leave the trap, the measurements are necessarily averaged over hundreds of lattice periods.

The circular cross-section of the PTSX electrodes allows the time-dependent electric potential to be calculated analytically [14]. Near the axis, the potential is quadrupolar and the average smooth focusing frequency of particles' transverse oscillations can be expressed for an applied voltage $V_0(t) = V_{0\max}\sin(2\pi f t)$ as

$$\omega_q = \frac{8e_b V_{0\max}}{m_b r_w^2 \pi^2 f 2^{3/2}}. \quad (1)$$

The confining force must balance both the thermal pressure force of the charge bunch and its space-charge force. For a Maxwellian thermal equilibrium distribution, the global force balance equation can be written as [1]

$$m_b \omega_q^2 R_b^2 = 2kT + \frac{N_b e_b^2}{4\pi\varepsilon_0}, \quad (2)$$

where R_b is the root-mean-squared (rms) radius of the charge bunch, kT is the transverse temperature, and N_b is the line density.

3. Injection mismatch

Experiments performed on PTSX that explore the effects of beam mismatch ought to begin with a steady-state trapped one-component plasma that corresponds to a matched beam so that the initial state is well known and well characterized. Subsequently, the applied voltage waveform can be modified in order to create a mismatch. However, it is observed in PTSX that a mismatch can exist before the plasma is trapped. During plasma injection, there can be a mismatch between the plasma emerging from the ion source and the transverse focusing lattice created by the applied voltage waveform.

Consider that the ion source is injecting a plasma with a circular, stationary cross-section into a transverse confinement system in which the matched state has a pulsating elliptical beam envelope. Therefore, the injected plasma is mismatched to the focusing lattice. Given the design of the PTSX ion source, this type of mismatch is inherent, but it presents an important opportunity to study sudden beam mismatch.

However, it is important to recognize that this injection mismatch can be minimized. When the smooth-focusing model is applicable, the transverse confinement is represented by an azimuthally symmetric, linear, radial restoring force. In this case, the smooth-focusing, matched beam envelope is in fact a circular, stationary envelope. Therefore, it should be possible to choose the applied voltage waveform and frequency to create a transverse confinement lattice in which the global force balance equation (Eq. (2)) is satisfied for a plasma with rms radius and temperature similar to the ion source.

This smooth-focusing injection mismatch is observed in experiments in which the ion source injects enough plasma that the equilibrium radius of the plasma (given the applied voltage waveform and frequency) is larger than the radius of the ion source. To best measure this effect by minimizing the relaxation of the plasma to an equilibrium radial profile, PTSX is operated in a single-pass mode where the confining electrodes at the diagnostic end of the device do not trap the plasma axially. Ions travel from the ion source to the diagnostic in a single transit of the machine.

The data and simulation results in Fig. 2 show the steady-state average radial profile for a case in which $\omega_q = 6.5 \times 10^4\,s^{-1}$, the vacuum phase advance is 50°, and the ion source is injecting enough plasma to create a plasma that, when trapped, corresponds to a normalized intensity of $s \sim 0.6$. The "shoulder" in the radial profile at $r = 3$ cm is the result of halo particles produced by the initial mismatch. The radial position of the shoulder scales with ω_q as expected; when ω_q is increased, the shoulder moves towards the axis, and when ω_q is decreased, the shoulder moves outwards. These types of radial profiles exhibiting halo particle production arising from mismatch were seen previously by Allen et al. [22]. This mismatch, when the plasma is trapped, causes these plasmas to have radial profiles that have super-Gaussian tails.

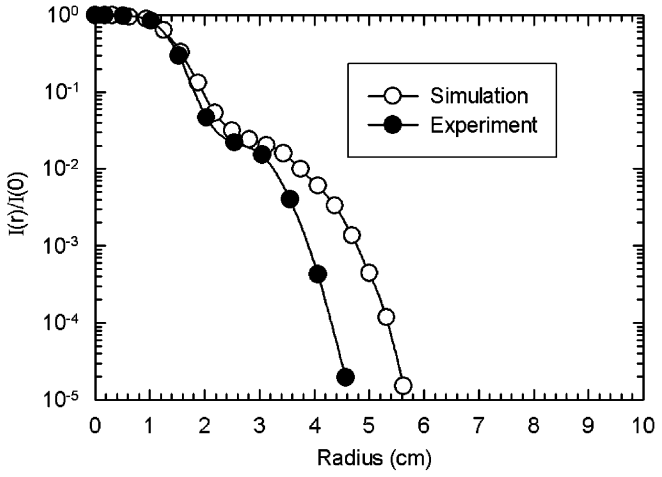

Fig. 2. The radial profile of the axial current streaming from the ion source to the collector exhibits a shoulder corresponding to the presence of halo particles in both PTSX experiments and 3D WARP PIC simulations when the ion source is poorly matched to the transverse confinement lattice.

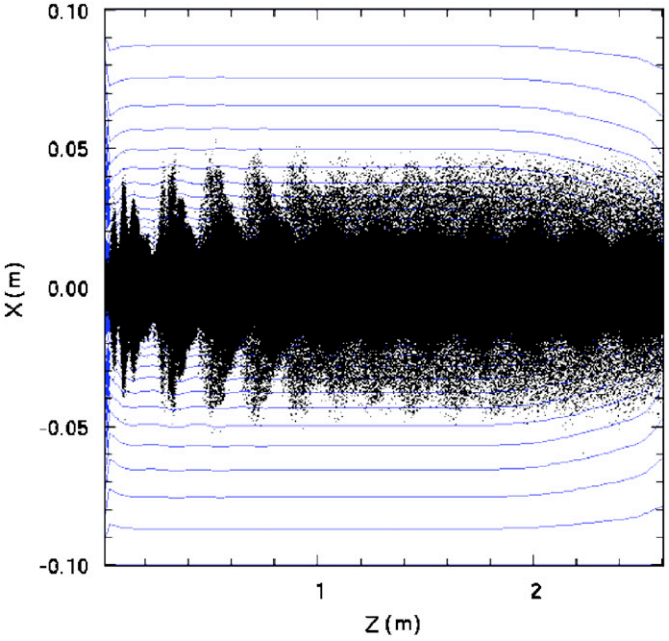

Fig. 3. The 3D WARP PIC simulation of mismatched injection shows both rapid and slow oscillations with frequencies f and ω_q near $z = 0$. For larger z, the mismatch-induced oscillations damp away, leaving a broad, diffuse halo around the central core.

Halo generation is also seen in 3D WARP PIC simulations. In the single-pass mode, the time-varying applied voltage waveform is mapped onto a z-varying beam envelope because there is minimal axial coupling of the plasma ions. The simulation results shown in Fig. 3 show that near the ion source at $z = 0$, the initial mismatch appears as large-amplitude envelope oscillations. Note from Fig. 3 that there are oscillations at both the applied frequency f and the smooth focusing frequency ω_q.

The distribution relaxes as the particles move downstream, and when $z > 1$ m, the transverse density profile of the plasma consists of a core that oscillates with frequency ω_q, and exhibits a broad diffuse halo.

The simplest way to minimize injection mismatch is to inject less plasma so that the expected equilibrium radius of the plasma is nearly equal to the radius of the ion source. It is found that well-matched plasmas with $s \sim 0.2$ can be created and trapped with minimal smooth-focusing injection mismatch. These plasmas serve as the baseline case for subsequent experiments on beam mismatch induced by applied voltage waveform modifications.

4. Injection optimization

In order to create well-matched plasmas in PTSX with $s \sim 0.2$, special care must be taken when injecting the plasma into the trap. It is found that it is optimal to inject plasma for slightly less than the round-trip transit time of ions in the trap and, further, to inhibit ion injection for a brief time before closing the injection electrodes and trapping the plasma.

Both considerations arise out of the need to minimize the number of particles present in the vicinity of the injection electrodes when the electrodes are switched from the fully oscillating voltage waveform to their static trapping voltage. Ions that are near the injection electrodes at the time trapping begins are boosted up to high potential energy—nearly the potential energy applied to the trapping electrodes. These "high-energy" particles can then stream along the length of the trap, and some may break through the trapping barrier on the dumping end of PTSX and be recorded by the collector diagnostic.

Particles that are leaving the ion source, or particles that have made a round-trip transit of the machine and have returned to the area near the ion source can be boosted to high-energy. Briefly inhibiting ion injection with a retarding bias applied to the acceleration grid allows the already-injected ions to move away from the injection region. Keeping the total injection time less than a round-trip transit time for the ions minimizes the number of ions that have returned to the injection region. Although some high-energy particles make only one transit through the machine and escape out the end, there are some that cannot escape through the axial trapping potential, and they may interfere with the transverse dynamics of the majority population of low-energy trapped particles. The result, whether the high-energy particles are trapped or not, is a distortion of the measured radial density profile.

The data in Fig. 4 demonstrate that if the ion injection is inhibited for at least 0.2 ms then the number of ions that overcome the axial trapping potential is minimized. The data in Fig. 5 demonstrate that the number of ions that break through the axial trapping potential increases if the total injection time is greater than about 1.9 ms. This is consistent with the round-trip transit time estimate of 1.85 ms, given the 3 V ion source bias voltage. Therefore, for the experimental results presented in this paper, the total injection time is chosen to be 1.7 ms, and the ion source injection is inhibited for 0.3 ms.

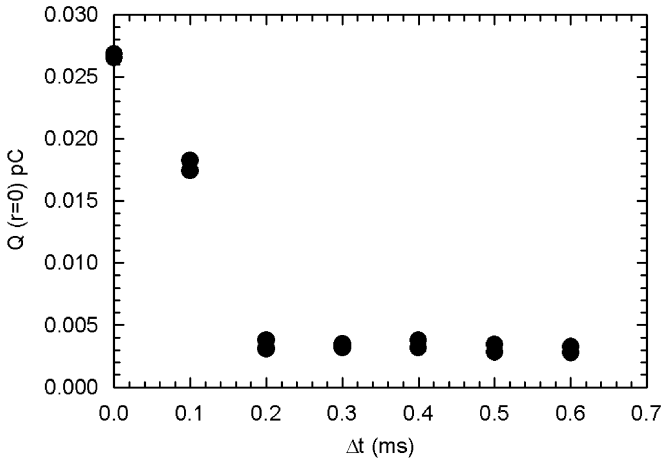

Fig. 4. Unless the ion source emission is inhibited for at least 0.2 ms, there are ions near the injection electrodes when the electrodes are switched to the axial trapping voltage $\hat{V}$. These ions acquire large kinetic energies and can escape and be collected even when the dumping electrodes are not opened.

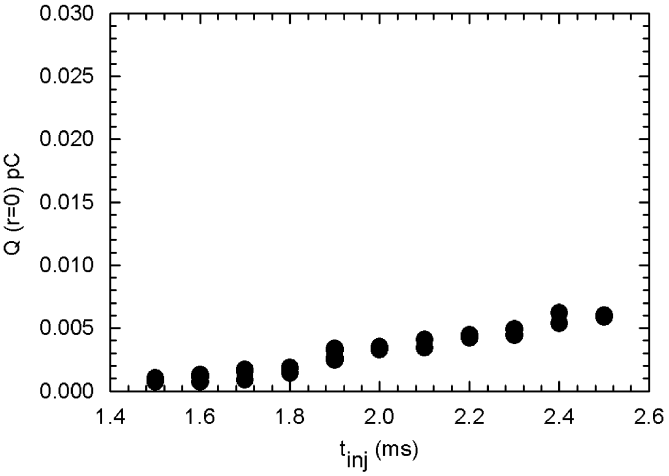

Fig. 5. If the total injection time is greater than 1.9 ms, then ions have enough time to make a round-trip transit and return to the vicinity of the injection electrodes. These ions acquire large kinetic energies and can escape and can be collected even when the dumping electrodes are not opened.

The plasma is allowed to relax for several milliseconds before changes to the applied voltage waveform are made. This relaxation time allows the residual mismatch oscillations due to the circular shape of the ion source to dissipate. As shown in Fig. 6, the relaxation time is approximately 6 ms. The radial density profile of the trapped plasma after 12 ms is nearly Gaussian (Fig. 7), as expected for a thermal equilibrium distribution corresponding to moderately low space-charge intensity. The transverse temperature inferred from global force balance

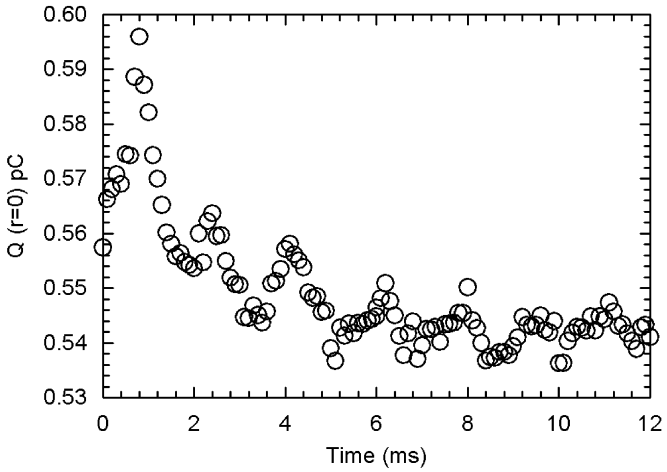

Fig. 6. When the injection conditions are optimized, the circular beam from the ion source is still mismatched to the oscillating quadrupole transverse confinement lattice. The subsequent mismatch oscillations damp away in several milliseconds.

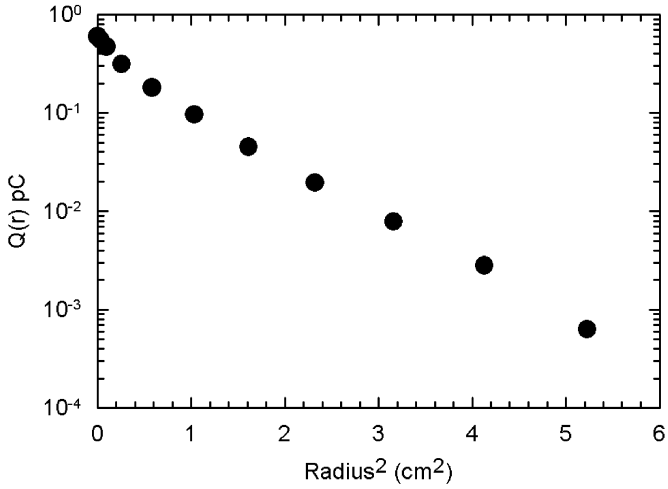

Fig. 7. After the injection conditions are optimized and the plasma relaxes for 12 ms, the transverse density profile is approximately Gaussian.

is $kT = 0.14\,\mathrm{eV}$, which is consistent with the thermal temperature of the cesium ion source.

5. Voltage waveform amplitude changes

Voltage waveform amplitude changes at fixed frequency correspond to quadrupole magnet strength changes at fixed magnet spacing. The transverse focusing frequency ω_q scales like V/f so that when the voltage waveform amplitude is increased, the plasma is compressed; and when the voltage waveform amplitude is decreased, the plasma expands. Transition rates ranging from instantaneous changes to adiabatic changes are studied by describing the envelope of the voltage by a hyperbolic tangent function with a variable "time constant". It is found that, if the amplitude change is less than 20%, there is little difference between the initial and final state for instantaneous and adiabatic changes. Further, for amplitude increases of up to 90%, a so-called adiabatic change can be made by changes in the voltage amplitude over only several lattice periods.

In the present experiments, the ratio of final to initial voltage amplitudes, V_f/V_i, is scanned from 0.1 to 2.2. For the data shown in Fig. 8, the voltage change is either made instantaneously, or over approximately 40 lattice periods. The plasma is dumped immediately after the transition is completed. It is clear that in the range $0.9 < V_f/V_i < 1.2$, there is no noticeable difference in the on-axis plasma density between the instantaneous and adiabatic cases. In fact, the radial density profiles for the instantaneous and adiabatic cases, where $V_f/V_i = 1.2$, are indistinguishable, and are both nearly Gaussian (Fig. 9). This suggests that modest changes in lattice strength may be made abruptly, without the need for a lengthy gradual-transition region. In contrast, for the case with $V_f/V_i = 1.9$, there is a 30% difference in the on-axis plasma density between the instantaneous and adiabatic cases. While the adiabatic change results in a radial density profile that is nearly Gaussian, the instantaneous change leads to a radial density profile that exhibits a broad halo region (Fig. 10), and has 10% fewer particles than the adiabatic case.

The choice of 40 lattice periods over which to make the adiabatic transitions was made to ensure that the transitions were sufficiently gradual. A variation of the number of transition lattice periods reveals that for voltage increases of 20%, 50% and 90%, the compression leads to an increase in the on-axis plasma density that maximizes after the transition is made in about four lattice periods. There is no extra benefit to be gained in density compression by making the transition more gradual than approximately four lattice periods.

Simulations made with a 2D version of the WARP code are in excellent agreement with these observations. Fig. 11

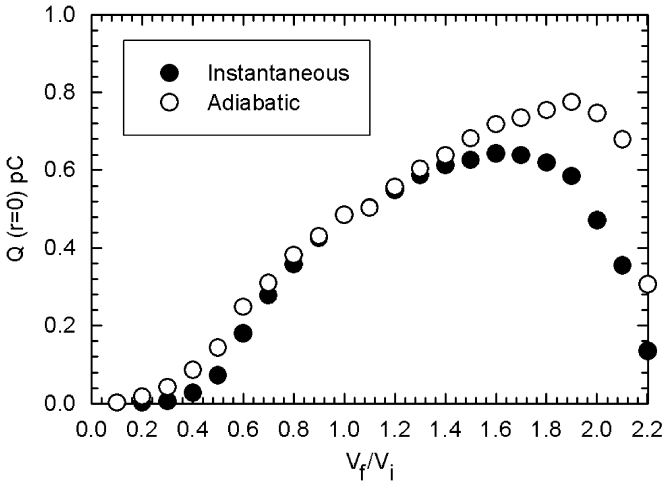

Fig. 8. Both sudden and adiabatic increases (decreases) in the voltage waveform amplitude cause the plasma to compress (expand) in the transverse plane.

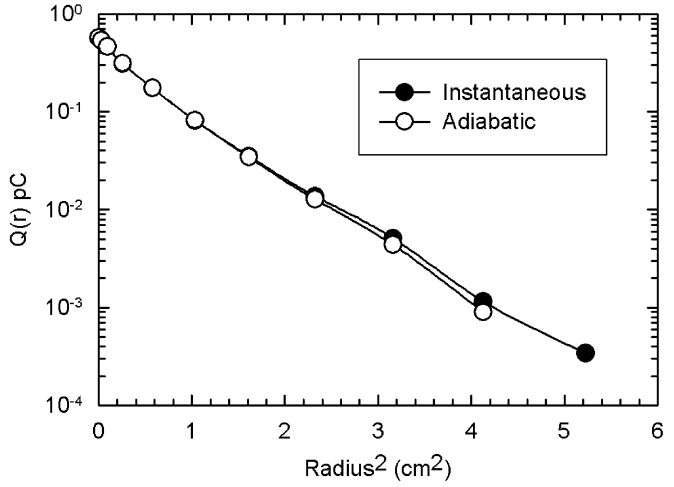

Fig. 9. For a voltage waveform increase of 20%, the change may be applied either instantaneously or adiabatically while still leaving the radial density profile nearly Gaussian.

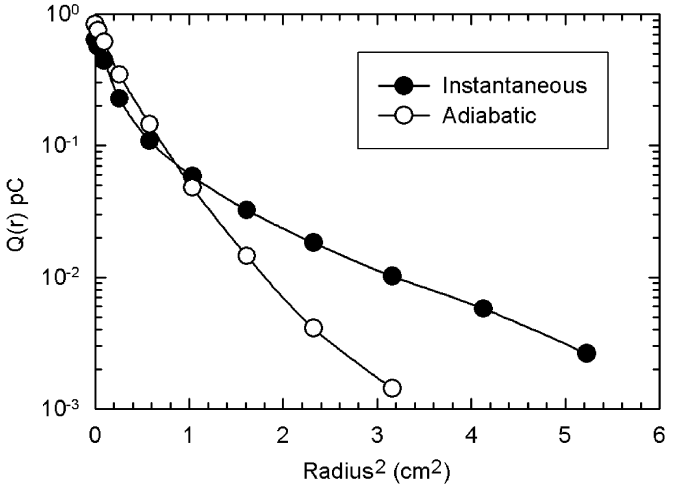

Fig. 10. For a voltage waveform increase of 90%, the adiabatic transition leaves the radial density profile nearly Gaussian. The instantaneous increase of 90% ultimately expels many particles into a halo region at large radius.

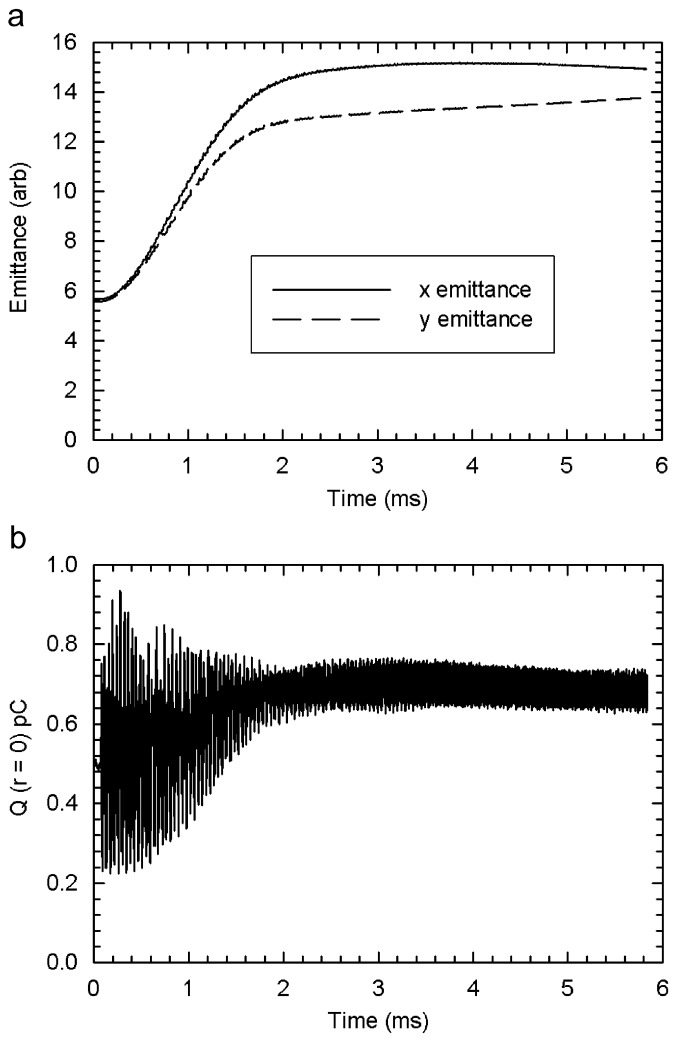

Fig. 11. 2D WARP PIC simulations for an instantaneous increase in the voltage waveform amplitude of 90% show that: (a) the transverse emittance more than doubles and (b) the beam becomes badly mismatched before relaxing to a matched final state after approximately 2 ms.

shows the transverse emittance and the on-axis plasma density as functions of time for a sudden increase in voltage amplitude of 90%. Even though the on-axis plasma density increases and eventually equilibrates as the beam reaches a matched state, the emittance more than doubles. However, if the transition is made over four lattice periods, then the simulation results in Fig. 12 show an even larger increase in on-axis plasma density, whereas the emittance changes by less than 1%.

It was noted previously that the plasma is dumped immediately after a transition is completed. However, if the transition puts the plasma into a transient state that ultimately relaxes into a near-equilibrium state, then the measured signal will be affected, since the measured signal is necessarily averaged over many lattice periods. This type of transient can be seen in Fig. 11(b) where, for the first 2.5 ms, the on-axis plasma density oscillates about values not equal to the asymptotic value at 6 ms. Similar to the residual mismatch oscillations shown in Fig. 6, it is expected from both the simulations and the experimental observations that these typical transient states last for several milliseconds.

It is therefore interesting to consider the difference between instantaneous and adiabatic changes in voltage amplitude when the amount of time that the plasma is held after the transition is increased. In the case of adiabatic transitions, the plasma should remain in a near-equilibrium state throughout the transition, and increasing the hold time should not change the result of the measurement. Instantaneous changes introduce the possibility of transient behavior after the transition, and so a change in the measured signal might be expected when the holding time is increased.

The experimental data in Fig. 13 show that for adiabatic changes with $V_f/V_i > 1$, there is no difference in the on-axis

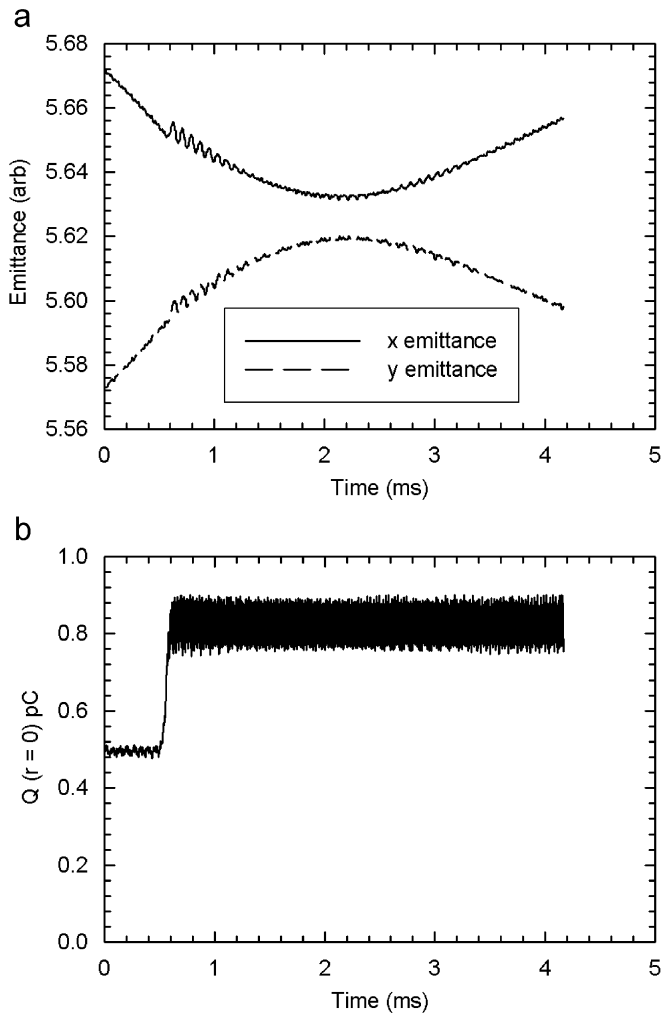

Fig. 12. 2D WARP PIC simulations for a smooth increase in the voltage waveform amplitude of 90% over only four lattice periods show that: (a) the transverse emittance changes by less than 1% and (b) the beam stays well matched.

plasma density when the plasma holding time is increased by up to 13 ms after the transition. However, contrary to expectations, for $V_f/V_i<1$, increasing the plasma holding time by up to 13 ms shows that the on-axis density continues to decrease with time after the transition.

For the instantaneous changes with $V_f/V_i>1$ in Fig. 13, increasing the holding time by up to 13 ms after the transition only slightly increases the measured on-axis density. This suggests that the transient that is induced by the sudden change in voltage amplitude is an oscillation that is nearly centered about the ultimate matched-state value. This slight increase in on-axis density is reproduced with good quantitative agreement by 2D WARP PIC simulations. For $V_f/V_i<1$, increasing the plasma holding time by up to 13 ms shows that the on-axis density continues to decrease for several milliseconds. Unlike in the adiabatic case for $V_f/V_i<1$, the continued decay in on-axis density for the instantaneous case with $V_f/V_i<1$ is in qualitative agreement with the 2D WARP PIC simulations.

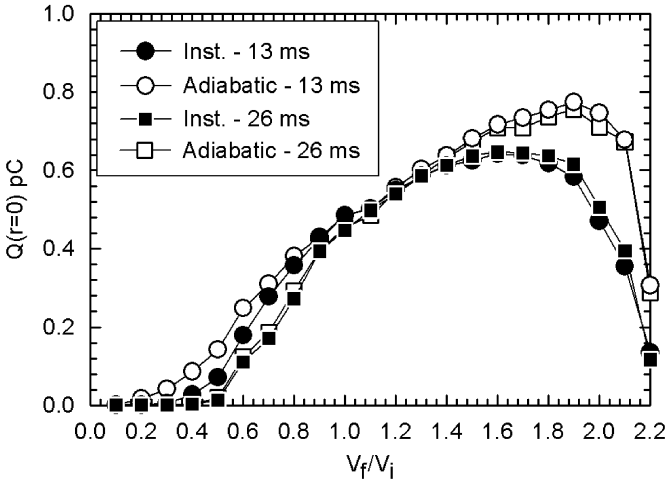

Fig. 13. For $V_f/V_i>1$, waiting an additional 13 ms does not affect the measured signal after an adiabatic transition, while after an instantaneous transition, the signal is slightly larger. For $V_f/V_i<1$, the signal decreases with increased hold time.

6. Conclusions

The PTSX is a compact and flexible laboratory facility for performing experiments on the long-distance propagation of intense charged particle beams. Injecting too much plasma creates a mismatch between the plasma and the transverse confinement lattice, and the resultant radial density distribution contains a significant population of halo particles. By reducing the amount of plasma injected, and by optimally timing the injection and trapping of the plasma, the number of halo particles in the initial trapped plasma can be minimized. The resulting well-matched plasma with $s\sim0.2$ can then be perturbed by applying voltage waveform amplitude changes. Changes of $\pm20\%$ compress or expand the beam slightly, but making the change adiabatically is unnecessary. Most interestingly, when the voltage waveform amplitude increases are larger than 20%, making the transition smoothly over only four lattice periods is sufficient to ensure that the beam remains well matched after the transition.

Acknowledgment

This research was supported by the US Department of Energy.

References

[1] R.C. Davidson, H. Qin, Physics of Intense Charged Particle Beams in High Intensity Accelerators, World Scientific, Singapore, 2001.
[2] M. Reiser, Theory and Design of Charged Particle Beams, Wiley, New York, 1994.
[3] A.W. Chao, Physics of Collective Beam Instabilities in High Energy Accelerators, Wiley, New York, 1993.
[4] P.G. O'Shea, M. Reiser, R.A. Kishek, S. Bernal, H. Li, M. Pruessner, V. Yun, Y. Cui, W. Zhang, Y. Zou, et al., Nucl. Instr. and Meth. Phys. Res. A 464 (2001) 646.

[5] N. Kjærgaard, M. Drewsen, Phys. Plasmas 8 (2001) 1371.
[6] Proceedings of the 2003 Particle Accelerator Conference, IEEE, Piscataway, NJ, 2003, IEEE Catalog Number 01CH37423, pp. 1–3571.
[7] Proceedings of the International Heavy Ion Fusion Symposium, Nucl. Instr. and Meth. Phys. Res. A (2005) 1.
[8] S.M. Lund, B. Bukh, Annu. Rev. Astron. Astrophys. 7 (2004) 024801.
[9] L.K. Spentzouris, J.-F. Ostiguy, P.L. Colestock, Phys. Rev. Lett. 76 (1996) 620.
[10] D. Neuffer, E. Colton, D. Fitzgerald, T. Hardek, R. Hutson, R. Macek, M. Plum, H. Thiessen, T.-S. Wang, Nucl. Instr. and Meth. Phys. Res. A 321 (1992) 1.
[11] J. Byrd, A. Chao, S. Heifets, M. Minty, T.O. Raubenheimer, J. Seeman, G. Stupakov, J. Thomson, F. Zimmerman, Phys. Rev. Lett. 79 (1997) 79.
[12] M. Dorf, R.C. Davidson, E.A. Startsev, Phys. Rev. ST Accel. Beams 9 (2006) 034202.
[13] W. Paul, H. Steinwedel, Z. Naturforsch. A 8 (1953) 448.
[14] R.C. Davidson, H. Qin, G. Shvets, Phys. Plasmas 7 (2000) 1020.
[15] H. Okamoto, H. Tanaka, Nucl. Instr. and Meth. Phys. Res. A 437 (1999) 178.
[16] A. Friedman, D.P. Grote, I. Haber, Phys. Fluids B 4 (1992) 2203.
[17] E.P. Gilson, R.C. Davidson, P.C. Efthimion, R. Majeski, H. Qin, Laser Part. Beams 21 (2003) 549.
[18] E.P. Gilson, R.C. Davidson, P.C. Efthimion, R. Majeski, H. Qin, in: Proceedings of the 2003 Particle Accelerator Conference, IEEE, Piscataway, NJ, 2003, IEEE Catalog No. 03CH37423C, p. 2655.
[19] E.P. Gilson, M. Chung, R.C. Davidson, P.C. Efthimion, R. Majeski, E.A. Startsev, Nucl. Instr. and Meth. Phys. Res. A 544 (2005) 171.
[20] E.P. Gilson, R.C. Davidson, P.C. Efthimion, R. Majeski, E.A. Startsev, AIP Conf. Proc. 692 (2003) 211.
[21] E.P. Gilson, R.C. Davidson, P.C. Efthimion, R. Majeski, Phys. Rev. Lett. 92 (2004) 155002.
[22] C.K. Allen, K.C.D. Chan, P.L. Colestock, K.R. Crandall, R.W. Garnett, J.D. Gilpatrick, W. Lysenko, J. Qiang, J.D. Schneider, M.E. Schulze, R.L. Sheffield, H.V. Smith, T.P. Wangler, Phys. Rev. Lett. 89 (2002) 214802.